Lin et al. *NPG Asia Materials* (2023) 15:13
https://doi.org/10.1038/s41427-022-00440-1

NPG Asia Materials

ARTICLE Open Access

Gyroid-structured nanoporous chitosan from block copolymer template for UVC reflection

Tze-Chung Lin[1], Chih-Ying Yang[2], Tsung-Lun Lee[1], Jheng-Wei Lin[1], Yu-Ting Liang[1], Yi-Ting Xie[1], Zhi-Hong Xie[2], Yu-Chueh Hung[2] and Rong-Ming Ho[1]

Abstract

Bioinspired from structural coloration of butterfly wing structure, this work aims to fabricate nanoporous chitosan for UVC reflection. By taking advantage of self-assembled polystyrene-*b*-polydimethylsiloxane (PS-*b*-PDMS) with double gyroid texture followed by hydrofluoric acid etching of PDMS block, nanoporous PS with well-defined nanochannels can be fabricated, and used as a template for templated crosslinking reaction of chitosan through a multiple pore-filling process. Well-ordered nanoporous chitosan with shifting networks in nanoscale can be successfully fabricated after removal of the PS template. With the low absorption of chitosan in the ultraviolet region and the shifting networks for opening the bandgap, it is appealing to exploit the nanonetwork chitosan as high reflective materials for UVC optical devices, as evidenced by finite-difference time-domain (FDTD) simulation and optical measurements experimentally.

Introduction

Observing the amazing creatures from nature, species such as butterflies exhibit beautiful colors on their wings; those colors are mainly attributed to the optical properties of photonic crystals within their constituent structures of the wings[1–9]. Among different photonic crystal systems of butterflies, single gyroid structure can be found in the families of *Papilionidae* and *Lycaenidae*, giving structural coloration[10–12]. For the single gyroid in butterflies' wings, it is originally obtained from the self-assembly of triblock or pentablock copolymers that gives double gyroid[11,13]; with the morphological evolution of millions years, a single gyroid can be formed by a series of degradation and oxidation to acquire the high reflectivity[14]. Most intriguingly, despite the typical quasi-ordered feature of the structure (the orientations are not aligned homogeneously), three-dimensional (3D) photonic crystals found in natural species still give conspicuous structural colors[14–17]. Chitin, the common constituted material of the butterfly wing, have been exploited in many industrial fields such as food and medicine, wound caring, tissue engineering and sensing[18–22]. Owing to the extreme stability of chitin in common solvent, how to process chitin for applications remains challenging. As a result, chitosan (deacetylated from chitin) which can be slightly dissolved in acidic water is much more favored due to its feasibility for processing into desired morphologies[23].

Bottom-up approaches such as synthetic block copolymers (BCPs) with the ability to self-assemble into spectacular nanonetwork structures, in particular gyroid structure, have been demonstrated as an emergent means for the fabrication of 3D photonic crystals with the length scales analog to wavelengths in visible to UV light region[24,25]. Yet, those bottom-up approaches face tremendous challenges of sliver window in phase diagram for network phase formation fabricating in cost-effective ways[26,27]. Note that it is feasible to acquire single gyroid by selective removal of one of networks from self-assembled triblock copolymers, such as PI-*b*-PS-*b*-PEO and PI-*b*-PS-*b*-PLA[28,29]. Yet, the synthesis of triblock

Correspondence: Yu-Chueh Hung (ychung@ee.nthu.edu.tw) or Rong-Ming Ho (rmho@mx.nthu.edu.tw)
[1]Department of Chemical Engineering, National Tsing Hua University, Hsinchu 30013, Taiwan, Republic of China
[2]Institute of Photonics Technologies, National Tsing Hua University, Hsinchu 30013, Taiwan, Republic of China
These authors contributed equally: Tze-Chung Lin, Chih-Ying Yang.

copolymer is not easy, which requires precision synthesis for the control of volume fraction of constituted blocks to acquire network phases; also, the phase behaviors will be extremely complicate. On the contrary, one can easily acquire network phases from self-assembled PS-*b*-PDMS by solution casting using selective solvent due to its high-χ character[30,31]. By taking advantage of network shifting after removal of matrix, it is feasible and facile to acquire network structure with single-gyroid-like photonic properties from diblock copolymer; that is a cost-effective method as compared to the one from triblock copolymer. With the degradable character of constituted components, well-ordered nanoporous polymers could be fabricated from BCP with gyroid-structured nanochannels as templates by selective degeneration of constituted blocks in the BCP[32–38]. Most importantly, the forming networks from original coherent networks in double gyroid would shift randomly toward each other after removal of the PS matrix, resulting in unique shifting-network structure[39]. This shifting-network structure can be referred to shifting-gyroid structure, which gives a single gyroid-like diffraction instead of double gyroid diffraction under scattering. Consequently, this shifting-network structure can give appealing optical activities, such as partial bandgap and topological effects, giving a feasibility of fabricating synthetic photonic crystals in cost-effective way[40]. Note that, generally, if the feature size of the structure is comparable to the wavelength of incident light, the structured materials with ordered texture may give high reflectance in accordance with specific wavelength; that is referred as photonic crystals[41,42]. By contrast, while the feature size (pore size or domain spacing) of the structure is smaller than the wavelength of incident light, the structured materials might give anti-reflective character; that is referred as optical metamaterials with subwavelength properties[38,43].

Biomimicking from butterfly wing structure, this work aims to fabricate high reflectance materials in UVC region at which the responsive wavelength is comparable to the interdomain spacing of the gyroid texture; that is a cost-effective method as compared to the one from high Mn dibock copolymers and triblock copolymers. As reported by our group, gyroid-structured polystyrene-*block*-polydimethylsiloxane (PS-*b*-PDMS) can be simply acquired from an originally symmetric composition in volume fraction for constituted blocks through solution casting by using a PS selective solvent[30,44]. Moreover, it is necessary to have the materials with low absorption for high reflectance; there are only a few materials possessing low absorption in the UVC region. Chitosan is one of the materials that is suitable to serve the purposes with low absorption and reasonably high dielectric contrast to provide the required photonic properties. Owing to the low solubility of chitosan, one-step process is impractical to complete the aimed templated synthesis for replication of the template texture. To completely pore fill the template, a multiple pore-filling process was thus developed, and the aimed replication could be achieved by templated crosslinking as demonstrated. As illustrated in Fig. 1, the PS template, fabricated from the

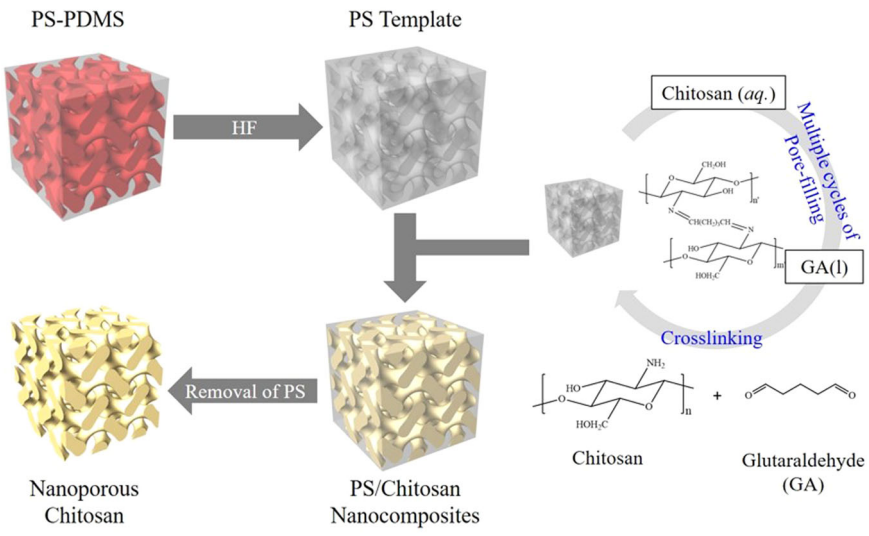

Fig. 1 Schematic illustration of fabricating gyroid-structured nanoporous chitosan. Solution-cast PS-*b*-PDMS with gyroid-texture is first treated with hydrofluoric acid aqueous solution to etch the PDMS block. After degeneration of the PDMS, nanoporous PS with gyroid-structured nanochannels can be obtained. Subsequently, chitosan aqueous solution with the crosslinking agent is pore-filled into the PS template through multiple pore-filling process, giving gyroid-structured PS/chitosan nanocomposites. After removal of the PS template, well-ordered chitosan with gyroid-structured nanonetworks can be fabricated.

self-assembly of PS-*b*-PDMS followed by hydrofluoric acid etching of PDMS, is pore-filled by immersing into acetic acid aqueous solution of chitosan. Considering the relatively low solubility of chitosan (2 wt%), it is impractical to achieve complete pore-filling through a single-step process. To address this problem, a crosslinking agent, glutaraldehyde (GA), is introduced for templated crosslinking of the chitosan to give the feasibility for multiple pore-filling process for achieving complete-filled chitosan to preserve the template structure. Subsequently, after removal of the PS template, nanoporous nanonetwork chitosan with gyroid texture can be fabricated. To our knowledge, this would be the first example to fabricate well-ordered nanonetwork chitosan, giving single-gyroid-like photonic behaviors. The suggested photonic behaviors for the optical performance of nanonetwork-structured chitosan with single gyroid-like optical characters are demonstrated by using finite-difference time-domain (FDTD) simulations and evidenced by optical measurements.

Methods and materials

Materials

PS-*b*-PDMS ($M_n^{PS} = 51{,}000$ gmol^{-1}, $M_n^{PDMS} = 35{,}000$ gmol^{-1}, $Đ = 1.03$, $f_{PDMS}{}^{v} \sim 0.42$ where $f_{PDMS}{}^{v}$ is the volume fraction of PDMS) was prepared by anionic polymerization as described in previous publication[44,45]. To prepare bulk sample with gyroid texture, PS-*b*-PDMS was dissolved in toluene at a concentration of 10 wt% in a vial, and then sealed well by aluminum foil with punch holes for evaporation of the solvent. Solution-cast sample was acquired by drying at ambient condition, following by drying in vacuum oven at 60 °C to remove residual solvent. To acquire nanoporous template, the gyroid-structured PS-*b*-PDMS was immersed in HF aqueous solution (HF/methanol = 1/3 by volume) for a week to ensure complete degeneration of PDMS block. After rinsing the HF-etched sample with a mixture of distilled water and methanol, nanoporous PS template with gyroid-structured nanochannels was obtained.

Fabrication of gyroid-structured chitosan with multiple pore-filling process

Chitosan was dissolved in pure acetic acid at a concentration of 2 wt% to form a solution with pH < 6 and filtrated through a filter with pore size of 0.45 μm to remove impurities. For pore-filling of chitosan, the nanoporous PS template was immersed in the chitosan solution with methanol as a surfactant for 30 min. The sample was then rinsed with ethanol to remove residual chitosan solution on sample surface. The rinsed sample was dried and transferred into solution of crosslinking agent, glutaraldehyde (GA), for 30 min to crosslink the chitosan molecules. Pore-filling process was completed after following the procedure above for multiple times. To remove PS template, the PS/chitosan nanocomposites were immersed in styrene solution for 12 h to ensure complete dissolution of PS template. Consequently, well-ordered gyroid-structured chitosan was obtained after drying in vacuum over night to remove residual styrene in the sample.

Transmission Electron Microscopy (TEM)

For the morphological observations by TEM, gyroid-structured PS/chitosan was prepared by microtoming. After OsO_4 staining for one day, a JEOL JEM-2100 LaB6 transmission electron microscope was used at an accelerating voltage of 200 kV.

Field-Emission Scanning Electron Microscope (FESEM)

For the morphological observations by FESEM, gyroid-structured chitosan was prepared after removal of PS template. A HITACHI SU8010 scanning electron microscope was used at accelerating voltages of 10–15 kV.

Small-angle X-ray Scattering (SAXS)

SAXS experiments were conducted at the synchrotron X-ray beam-line BL23A at the National Synchrotron Radiation Research Center (NSRRC) in Hsinchu to examine the forming gyroid structure of chitosan.

Optical measurements of gyroid-structured chitosan

To precisely control the thickness of the sample, Leica Ultramicrotome was used to acquire the microsections from bulk and the thickness was confirmed by single-spot thickness measurements. The film thickness was measured by a reflectometer (Filmetrics F20) which is available for thickness ranging from 15 nm to 70 μm. The microsections were transferred onto quartz substrate after microsectioning followed by UV degradation for 24 h for complete removal of the PS template as evidenced by FTIR measurements. The optical property of the fabricated gyroid-structured chitosan film was measured using a balanced deuterium halogen source (Ocean Optics DH-2000-BAL) as a broadband optical source with wavelength ranging from 230 nm to 2500 nm and a spectrometer (Ocean Optics USB 4000) coupled with a fiber (F600-UVVIS-SR) as a detector. The substrate with microsections of gyroid-structured chitosan was clamped on a substrate holder which was mounted on the XYZ linear translation stage and located between the light source and detector. The transmittance spectra were recorded by Ocean Optics Spectrasuite software with a 120 ms integration time.

Results and discussion

Gyroid-structured nanoporous chitosan *via* multiple pore-filling process

Following the well-established methods developed by our laboratory, gyroid-structured PS-*b*-PDMS could be

obtained from lamellae-forming PS-*b*-PDMS by casting of toluene (a PS-selective solvent) solution[44]. Nanoporous PS with gyroid-structured nanochannels could be fabricated after etching of PDMS in the PS-*b*-PDMS by using hydrofluoric aqueous solution (see Fig. S1 and SI for details), and then used as a template for templated crosslinking reaction of chitosan. Owing to the low solubility of chitosan, it is reasonable to expect that only small amount of chitosan could be crosslinked by glutaraldehyde. To increase the amount of chitosan pore-filling into the PS template, a multiple pore-filling process was introduced. After pore-filling of chitosan aqueous solution, the sample was transferred into dilute GA solution for crosslinking. Subsequently, the sample was rinsed to remove the residual crosslinked agent. This process was repeated several times until the PS template was fully pore-filled. After completion of crosslinking reaction, the pore-filled chitosan can thus be firmly formed within the template for the next cycle. The functional groups of NH_2 will partially convert to imine groups (C = N) after crosslinking, leading to the deposition of the chitosan within the PS template. Furthermore, unreacted NH_2 group can be used as a reactive site for crosslinking reaction in the consecutive pore-filling process (see Fig. S2 for the details of the crosslinking reaction). Figure S3 shows the TEM micrograph of PS/chitosan nanocomposites after different pore-filling cycles followed by templated crosslinking at which the bright microdomain is the PS and the dark microdomain refers to stained chitosan (C-O-C bond) by OsO_4. As shown in Fig. S3a, only a thin layer of chitosan could be found in the micrograph, indicating that only a small amount of chitosan deposited on the inner wall of the nanochannels. After five pore-filling cycles with templated crosslinking reaction (Fig. S3b), the formation of chitosan nanonetworks can be partially recognized. With the pore-filling cycles more than ten, as the one after fifteen cycles (Fig. S3c), a gyroid [110] projection with the connecting nanonetwork texture can be found, reflecting the formation of the gyroid-structured PS/chitosan nanocomposites. For comparison, the PS/chitosan nanocomposites were fabricated without using crosslinker. As shown in Fig. S4, only a small amount of chitosan could be deposited in the template. The morphological results indicate that the suggested multiple pore-filling process with the use of crosslinker indeed provides the feasibility for the fabrication of PS/chitosan nanocomposites.

The formation of gyroid-structured nanocomposites was further evidenced by 1D SAXS profiles. As shown in Fig. 2, characteristic reflections of a double gyroid structure at the relative q values of √6:√8:√16:√32:√40:√52 can be identified, suggesting the formation of gyroid-structured nanochannels in the PS. The inter-domain distance of (211) plane (d_{211}) of the gyroid was calculated

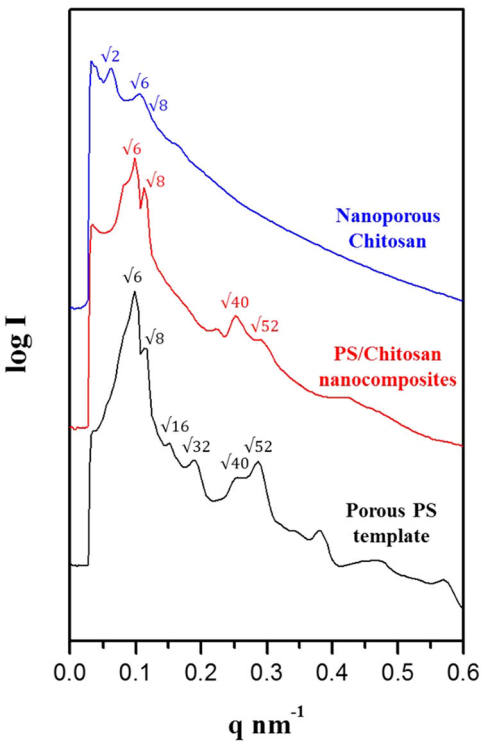

Fig. 2 1D SAXS profiles of the fabricated samples. 1D SAXS profiles of nanoporous PS template, gyroid-structured PS/chitosan nanocomposites, and chitosan nanonetworks after removal of PS template.

to be 61.2 nm from the primary peak, giving the lattice constant of 150 nm for a unit cell. After multiple pore-filling process, the reflections of the PS/chitosan nanocomposites at the relative q values of √6:√8:√40:√52 can then be identified, suggesting well preservation of double gyroid morphology after pore-filling followed by templated crosslinking reaction. In contrast to the PS/chitosan nanocomposites, an additional reflection at the low q region can be found after removal of PS template, giving the reflections at the relative q values of √2:√6:√8 for nanoporous chitosan. According to previous study, the appearance of the additional reflection (√2) is mostly attributed to the shifting of two coherent networks after removal of the template, resulting in the breaking of inversion symmetry of double gyroid phase[39]. The resultant structure in the sample thus leads to the similar X-ray scattering profile from single gyroid. To verify the suggested shifting network structure based on the diffraction results, the nanoporous chitosan fabricated was directly observed by FESEM. As shown in Fig. 3, chitosan nanonetworks can be found in the FESEM micrograph but unlike the typical double gyroid texture. Instead, the reposition of two frameworks both with trigonal planar networks can be clearly observed, giving a shifting

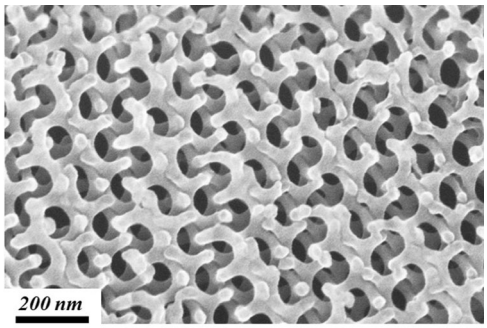

Fig. 3 Morphological characterization of the fabricated sample. FESEM micrograph of the gyroid-structured chitosan nanonetworks after removal of the PS template by using styrene monomer.

network structure. As shown in Fig. S5a, significant shifting of the dual networks can be found at which the red and blue trigonal planar junctions are lean by each other that breaks the inversion symmetry of double gyroid. On the other hand, Fig. S5b shows the shifting behavior of the nanonetworks along different direction, revealing that there are different degrees of shifting in various directions after removal of the PS template due to numerous grain boundaries in self-assembled BCP. Namely, the overall shifting behavior can be viewed as random shifting, resulting in the diffraction results similar to the one from single gyroid structure, which is in line with the SAXS results[39]. Unlike the butterfly wing structure (nanoporous chitin), which required specific enzymes for fabrication of nanonetworks followed by a series of chemical reduction to give single gyroid texture; in this study, a simple method was proposed to fabricate the one with single-gyroid-like structure by templated synthesis of chitosan followed by physical shifting after removal of the template. By taking advantage of the well-defined structure of the nanoporous PS template with the multiple pore-filling process for templated crosslinking reaction, this would be the first example to fabricate well-ordered chitosan with single-gyroid like nanonetworks. Following our previous study, interesting photonic crystal behaviors (i.e., partially-opened bandgap) can be acquired by using this shifting network structure for optical devices[39].

Photonic properties of chitosan nanonetworks

For the optical application of the well-ordered nanoporous chitosan fabricated, the first requirement is to have a low degree of absorption for the materials used. Figure S6a shows the transmittance spectrum of a chitosan film with a thickness of 1.5 μm from UV to visible region. Despite the fringe print profile due to thin-film interference, the chitosan film gives a transmittance level above 95% in a broad wavelength range above 230 nm to visible region; there is a significant decrease on the transmittance below 230 nm, which is attributed to the $n \rightarrow \sigma^*$ transitions of the auxochrome from the lone pair of amine group[46]. The high transmittance character indicates that chitosan is applicable to be a widely-used optical material, especially in UVC region. To further examine the expected performance as high reflectivity, the extinction coefficient and the refractive index of chitosan were measured by ellipsometer. As shown in Fig. S6b, the extinction coefficient of chitosan is below the order of 10^{-3} in the wavelength region from 230 nm to the visible region, implying an extremely low level of absorption. Below 230 nm, the absorption dramatically increases, which is in line with the transmittance measurements. The refractive index of chitosan exhibits a normal dispersion relation with wavelength, ranging from 1.55 at 360 nm to 1.61 at 235 nm. Note that the performance of reflection is strongly dependent upon the refractive index contrast (i.e., the dielectric constant contrast) with air. As a result, it is appealing to exploit the well-ordered chitosan nanonetworks fabricated as high reflective films in the UVC region. To demonstrate the feasibility of using the gyroid-structured nanoporous chitosan fabricated for optical applications, in particular for the performance of high reflective materials in UVC region, a series of simulations were carried out. The corresponding reflection spectra were simulated by using the software package of Lumerical Solutions based on the finite-difference time-domain (FDTD) method[47]. The analytical equation of the gyroid surface can be approximated by using following expression.

$$\mathrm{sinXcosY} + \mathrm{sinYcosZ} + \mathrm{sinZcosX} = \mathrm{t}$$

where $X = 2\pi x$, $Y = 2\pi y$, $Z = 2\pi z$, $|t| \le 1.413$. In this simulation, the volume fraction of the double gyroid is set to be 37% according to the fabricated sample, constructed by two intertwined single gyroid networks with a volume fraction of 18.5% ($t = \pm 0.958$). To systematically examine the optical properties of the shifting-gyroid networks, the double gyroid structure with different relative displacements between the two intertwined networks were constructed by applying a coordinate transformation to above equation. One network of the double gyroid networks is fixed while the other network is shifted along each axis in a Cartesian coordinate system. Figures S7a–c are the illustrations of the shifting networks with the displacements along *x*, *y*, and *z*-coordinates, respectively; note that the simulated results should be scalable. Structures with different amounts of shifting were acquired by setting different displacements in the range of ±0.5a. In our previous work, a random-shifting double gyroid structure with breaking symmetry can be achieved by subgroup symmetry operation, leading to the opening of bandgaps[39].

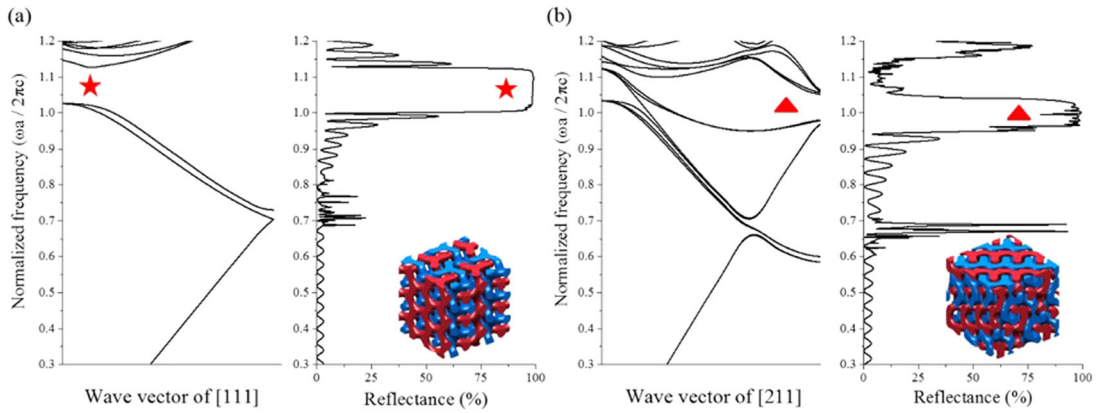

Fig. 4 Simulated photonic bandgap of gyroid-structured nanonetworks. The band structures and reflection spectra of fabricated gyroid-structured nanonetworks along **a** [111] and **b** [211] directions. The bandgap and corresponding high reflection areas are denoted by ★ and ▲, respectively. The inset figures are the illustrations of the double gyroid structures with specific orientations.

Similar behaviors were also reported in a shifting double-diamond titania scaffold[48]. Therefore, it is of great interest to examine the evolution of reflection properties when breaking the structure symmetry by introducing a displacement between two networks. Meanwhile, the fabricated nanonetwork chitosan films may consist of multiple domains with different orientations. Note that even without highly ordered structures, high reflection could still be achieved in an otherwise multi-domain structure from multiple grains with specific crystal orientations, similar to the scenario of coloration in many species[10–12]. For a gyroid-structured thin film from the self-assembly of BCPs, double gyroid with (211) plane parallel to surface is commonly found due to surface energy consideration[49,50]. Also, the gyroid-structured thin film with (111) plane can be frequently found in the examination of the structural coloration of butterfly wing[51,52]. We therefore simulated the reflection spectra of a finite gyroid slab along [211] and [111] directions as model systems for expected optical properties. Note that the coordinate of the above equation could be simply rotated by applying a 3D rotation matrix for the construction of double gyroid structure along arbitrary directions.

To yield high reflection along [211] and [111] directions, we first inspected the band structure without shifting to look for possible frequency ranges with high reflection in common. Figure 4a shows the band structure and the corresponding reflection spectrum along [111]. We found that there is a Bragg bandgap between the 3rd and 4th bands at $0.99 < \omega a/2\pi c < 1.11$ (denoted by ★), yielding a high reflection of ~100% in the spectrum. Figure 4b shows the band structure and reflection spectrum along [211] direction. There is a high reflectance band around the normalized frequencies of 0.95 ~ 1.05 (denoted by ▲). By comparing the reflection spectra in Fig. 4, a band of interest around a normalized frequency of 1.02 can be identified at which a high reflection band will be exhibited in both directions. A lattice parameter of 280 nm was used to demonstrate the feasibility of using the fabricated chitosan nanonetworks for high reflection band in the UV regime. Next, optical properties of the shifting double gyroid networks were examined. The reflection spectra were simulated with a thickness around 2 μm. Figure S8a shows the reflection spectra of [111] direction in which the shift is along x direction within a maximum shifting extent of ±0.2a. The high reflection band arising from Bragg resonance is centered around 265 nm, and only a slight change of bandwidth can be found under different shifting amounts. Figures S8b, c are the reflection spectra for shifting along *y* and *z*-directions, respectively. In general, the high reflection band can be maintained regardless of the displacement (degree of shifting) and shifting direction, suggesting that the reflection band along [111] is quite robust against the shifting of the network. Figures S8d–f show the reflection spectra of [211] with shifting along the *x*, *y*, and *z*-directions, respectively. A high reflection band centered at 280 nm with a bandwidth around 30 nm could be observed in all cases except for +0.2a shifting of x-direction, and only a slight change of bandwidth was found under different degrees of shifting amounts. The results indicate that the high reflection bands are quite robust in spite of the physical shifting after removal of the PS template, giving feasibility to achieve expected optical properties. To exemplify conditions of expected optical properties, a scenario where two domains with different orientations are adjacent in space was proposed for simulation. As shown in Fig. S9a, the simulated reflection spectra along (211) and (111) planes were presented separately, indicating that the reflection bands from these two planes locate at slightly different wavelength ranges. When these

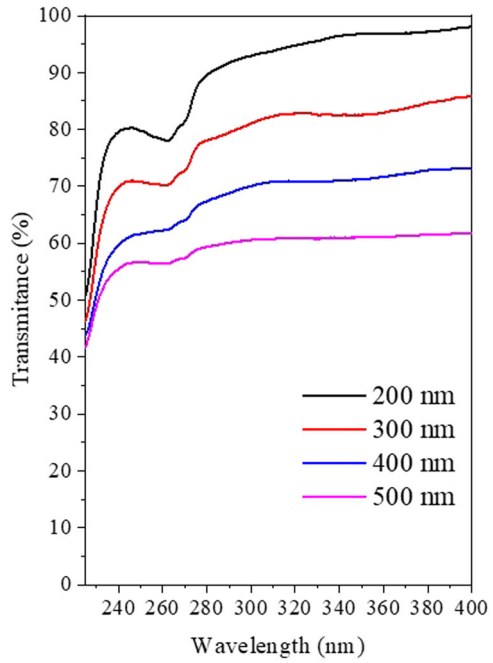

Fig. 5 Transmittance measurement of nanonetwork chitosan thin films. Transmittance spectra of gyroid-structured nanoporous chitosan monoliths fabricated with thickness ranging from 200 to 500 nm.

two domains are weighted by different compositions (volume ratios), as shown in Fig. S9b, reflection spectra of a slab consisting of two domains shows the collective optical response with the highest reflectance occurred at the wavelength where the original reflection spectra of these two planes overlap. It can also be inferred that the optical properties of the slab are mainly governed by the domain with a larger volume fraction. Consequently, the reflection properties of the shifting double gyroid slab could thus be tailored by domain spacing and orientation accordingly.

Optical measurements of gyroid-structured nanoporous chitosan

The thin-film samples with single-gyroid-like structured chitosan were characterized by optical measurements for examination of simulated photonic behaviors (see experimental section in detail). For the optical signal in UVC region, transmittance measurements with higher reliability were carried out using a broadband light source available at the current stage with a wavelength range down to 240 nm. As shown in Fig. 5, the transmittance levels were recorded for the nanonetwork chitosan fabricated with a thickness ranging from 200 to 500 nm. For the film with a thickness of 200 nm, the transmittance result exhibits a pronounced dip around 260 nm. With the increase of film thickness, the results show that the transmittance dip can still be persistently identified for the chitosan films though it becomes less pronounced due to increasing scattering level inevitably from grains with different orientations and boundaries of the fabricated samples. Note that by subtracting and scattering background and negligible absorption of chitosan, the transmittance dip can be viewed as reflection peak. To validate the photonic behaviors of chitosan with single-gyroid like structure from the observed transmittance dip at 260 nm, FDTD simulation was carried out for the fabricated samples. Given the lattice constant of 150 nm, as calculated from the SAXS results, the desirable high reflection bands attributed to [211], [111], and [110] directions are located at approximately 150 nm as predicted (Fig. S10a), which is outside the range of the device that could be reached at the current stage. On the other hand, the reflection bands at 220 nm and 260 nm can also be found, referring to the partially opened bandgaps of (211) and (110) planes at lower frequency (longer wavelength), respectively. Moreover, as shown in Fig. S10b, the reflection band of [110] at 260 nm can be tuned through various degree of network shifting, resulting in the enhancement of the reflectance. Consequently, the observation of transmittance dip at 260 nm is referred to the partially opened band gap along [110] direction whose Bragg bandgap located at normalized frequencies of 1.09 ~ 1.15, which is close to the high reflection bands of (211) and (110) planes. Note that the (110) plane may not be a predominant plane normal to the incident light in the nanonetwork chitosan fabricated; as a result, the reflectance result will be less significant than the simulation one with the scenario by assuming a monograin sample.

As evidenced by the expected optical signal and multi-domain scenario, it is promising to derive highly reflective chitosan nanonetworks with the character of low absorption in UVC region with appropriate tuning of the dimension of forming gyroid. By virtue of the low loss nature of chitosan in the UV region, the high reflection bands at lower wavelength could be red-shifted to desired wavelength range by further increasing the lattice constant of the gyroid-structured chitosan networks[5,52,53]. Some advanced approaches have been developed to control the domain spacing of gyroid block copolymer photonic crystal by solvent vapor annealing and selective solvent evaporation[54]. By tailoring the domain spacing and featuring the optical characteristics of the gyroid morphologies with different structural properties, the high-reflection wavelength range could be freely scaled to the band of interest. Such scalability of gyroid-structured chitosan networks provides a versatile route to achieve high reflection in the UV region and might find broad applications in optical devices for UV applications.

Conclusions

In conclusion, gyroid-structured nanoporous chitosan could be successfully fabricated for the first time by using a nanoporous polymer from the self-assembly of PS-*b*-PDMS followed by hydrofluoric acid etching of PDMS block as a template for templated crosslinking reaction. A process using multiple pore-filling cycles with the use of crosslinking agent was developed to achieve the fabrication of the well-ordered chitosan from templating. Bio-mimicking from the structural coloration of butterfly wing structure, the fabricated nanoporous chitosan with shifting gyroid-structured nanonetworks and extremely low absorption gives rise to the appealing applications as UV optical devices for high reflectance, in particular, in the deep UV region for the development of optical devices such as UV light emitting diodes (LEDs).

Acknowledgements

The authors would like to thank the National Science Council of the Republic of China, Taiwan, for financially supporting this research under Contract No. Grant NSC 106-2119-M-007-010- and National Synchrotron Radiation Research Center (NSRRC) for its assistance in the Synchrotron SAXS experiments.

Author contributions

T.C.L. and C.Y.Y. conceived and designed the experiments. T.C.L., J.W.L., Y.T.L., and Y.T.X. obtained experimental data. C.Y.Y. and Z.H.X. performed theoretical calculations. C.Y.Y. and T.L.L. analyzed the experimental and theoretical results. T.C.L. and C.Y.Y., and T.L.L. wrote the manuscript after discussion with all the authors. Y.C.H. and R.M.H. supervised the entire project.

Conflict of interest

The authors declare no competing interests.

Publisher's note

Springer Nature remains neutral with regard to jurisdictional claims in published maps and institutional affiliations.

Supplementary information The online version contains supplementary material available at https://doi.org/10.1038/s41427-022-00440-1.

Received: 30 August 2022 Revised: 8 September 2022 Accepted: 12 September 2022.
Published online: 31 March 2023

References

1. Ghiradella, H. Light and color on the wing: structural colors in butterflies and moths. *Appl. Opt.* **30**, 3492–3500 (1991).
2. Vukusic, P., Sambles, J. R., Lawrence, C. R. & Wootton, R. J. Quantified interference and diffraction in single Morpho butterfly scales. *Proc. R. Soc. B* **266**, 1403–1411 (1999).
3. Vukusic, P., Sambles, J. & Ghiradella, H. Optical classification of microstructure in butterfly wing-scales. *Photonics Sci. N.* **6**, 61–66 (2000).
4. Vukusic, P., Sambles, J. R. & Lawrence, C. R. Colour mixing in wing scales of a butterfly. *Nature* **404**, 457 (2000).
5. Maldovan, M., Urbas, A. M., Yufa, N., Carter, W. C. & Thomas, E. L. Photonic properties of bicontinuous cubic microphases. *Phys. Rev. B* **65**, 165123 (2002).
6. Urbas, A. M., Maldovan, M., DeRege, P. & Thomas, E. L. Bicontinuous cubic block copolymer photonic crystals. *Adv. Mater.* **14**, 1850–1853 (2002).
7. Galusha, J. W., Richey, L. R., Gardner, J. S., Cha, J. N. & Bartl, M. H. Discovery of a diamond-based photonic crystal structure in beetle scales. *Phys. Rev. E Stat. Nonlin. Soft Matter Phys.* **77**, 050904 (2008).
8. Kolle, M. et al. Mimicking the colourful wing scale structure of the Papilio blumei butterfly. *Nat. Nanotechnol.* **5**, 511–515 (2010).
9. Dolan, J. A. et al. Optical properties of gyroid structured materials: from photonic crystals to metamaterials. *Adv. Opt. Mater.* **3**, 12–32 (2015).
10. Michielsen, K., De Raedt, H. & Stavenga, D. G. Reflectivity of the gyroid biophotonic crystals in the ventral wing scales of the Green Hairstreak butterfly, Callophrys rubi. *J. R. Soc. Interface* **7**, 765–771 (2010).
11. Saranathan, V. et al. Structure, function, and self-assembly of single network gyroid ($I4_132$) photonic crystals in butterfly wing scales. *Proc. Natl Acad. Sci. USA* **107**, 11676–11681 (2010).
12. Wilts, B. D., Michielsen, K., De Raedt, H. & Stavenga, D. G. Iridescence and spectral filtering of the gyroid-type photonic crystals in Parides sesostris wing scales. *Interface Focus* **2**, 681–687 (2012).
13. Saranathan, V. et al. Structural diversity of arthropod biophotonic nanostructures spans amphiphilic phase-space. *Nano Lett.* **15**, 3735–3742 (2015).
14. Saranathan, V., Narayanan, S., Sandy, A., Dufresne, E. R. & Prum, R. O. Evolution of single gyroid photonic crystals in bird feathers. *Proc. Natl Acad. Sci. USA* **118**, e2101357118 (2021).
15. Vukusic, P. & Sambles, J. R. Photonic structures in biology. *Nature* **424**, 852–855 (2003).
16. Kinoshita, S., Yoshioka, S. & Miyazaki, J. Physics of structural colors. *Rep. Prog. Phys.* **71**, 076401 (2008).
17. Saranathan, V. et al. Structure and optical function of amorphous photonic nanostructures from avian feather barbs: a comparative small angle X-ray scattering (SAXS) analysis of 230 bird species. *J. R. Soc. Interface* **9**, 2563–2580 (2012).
18. Shahidi, F., Arachchi, J. K. V. & Jeon, Y. J. Food applications of chitin and chitosans. *Trends Food Sci. Technol.* **10**, 37–51 (1999).
19. Ravi Kumar, M. N. V. A review of chitin and chitosan applications. *React. Funct. Polym.* **46**, 1–27 (2000).
20. Rabea, E. I., Badawy, M. E., Stevens, C. V., Smagghe, G. & Steurbaut, W. Chitosan as antimicrobial agent: applications and mode of action. *Biomacromolecules* **4**, 1457–1465 (2003).
21. Kim, I. Y. et al. Chitosan and its derivatives for tissue engineering applications. *Biotechnol. Adv.* **26**, 1–21 (2008).
22. Muzzarelli, R. A. A. Chitins and chitosans for the repair of wounded skin, nerve, cartilage and bone. *Carbohydr. Polym.* **76**, 167–182 (2009).
23. Huang, G. et al. Fabrication of 3D photonic crystals from chitosan that are responsive to organic solvents. *Biomacromolecules* **15**, 4396–4402 (2014).
24. Bates, F. S. & Fredrickson, G. H. Block copolymer thermodynamics: theory and experiment. *Annu. Rev. Phys. Chem.* **41**, 525–557 (1990).
25. Bates, F. S. & Fredrickson, G. H. Block copolymers—designer soft materials. *Phys. Today* **52**, 32–38 (1999).
26. Park, M., Harrison, C., Chaikin, P. M., Register, R. A. & Adamson, D. H. Block copolymer lithography: Periodic arrays of similar to 10^{11} holes in 1 square centimeter. *Science* **276**, 1401–1404 (1997).
27. Ullal, C. K. et al. Photonic crystals through holographic lithography: Simple cubic, diamond-like, and gyroid-like structures. *Appl. Phys. Lett.* **84**, 5434–5436 (2004).
28. Epps, T. H. et al. Ordered network phases in linear poly(isoprene-b-styrene-b-ethylene oxide) triblock copolymers. *Macromolecules* **37**, 8325–8341 (2004).
29. Wang, H. F. et al. Networks with controlled chirality via self-assembly of chiral triblock terpolymers. *Sci. Adv.* **6**, eabc3644 (2020).
30. Lo, T. Y. et al. Phase transitions of polystyrene-*b*-poly(dimethylsiloxane) in solvents of varying selectivity. *Macromolecules* **46**, 7513–7524 (2013).
31. Chang, C. Y. et al. Mesoscale networks and corresponding transitions from self-assembly of block copolymers. *Proc. Natl Acad. Sci. USA* **118**, e2022275118 (2021).
32. Hashimoto, T., Tsutsumi, K. & Funaki, Y. Nanoprocessing based on bicontinuous microdomains of block copolymers: Nanochannels coated with metals. *Langmuir* **13**, 6869–6872 (1997).
33. Chan, V. Z. et al. Ordered bicontinuous nanoporous and nanorelief ceramic films from self assembling polymer precursors. *Science* **286**, 1716–1719 (1999).
34. Crossland, E. J. W. et al. A bicontinuous double gyroid hybrid solar cell. *Nano Lett.* **9**, 2807–2812 (2009).
35. Wang, Y. et al. Nanoporous metal membranes with bicontinuous morphology from recyclable block-copolymer templates. *Adv. Mater.* **22**, 2068–2072 (2010).
36. Hsueh, H. Y. et al. Nanoporous gyroid nickel from block copolymer templates via electroless plating. *Adv. Mater.* **23**, 3041–3046 (2011).
37. Li, F. et al. Highly porous metal oxide networks of interconnected nanotubes by atomic layer deposition. *Nano Lett.* **12**, 5033–5038 (2012).

38. Hsueh, H. Y., Yao, C. T. & Ho, R. M. Well-ordered nanohybrids and nanoporous materials from gyroid block copolymer templates. *Chem. Soc. Rev.* **44**, 1974–2018 (2015).
39. Hsueh, H. Y. et al. Shifting networks to achieve subgroup symmetry properties. *Adv. Mater.* **26**, 3225–3229 (2014).
40. Fruchart, M. et al. Soft self-assembly of Weyl materials for light and sound. *Proc. Natl Acad. Sci. USA* **115**, E3655–E3664 (2018).
41. John, S. Strong localization of photons in certain disordered dielectric superlattices. *Phys. Rev. Lett.* **58**, 2486–2489 (1987).
42. Yablonovitch, E. Inhibited spontaneous emission in solid-state physics and electronics. *Phys. Rev. Lett.* **58**, 2059–2062 (1987).
43. Hsueh, H. Y. et al. Inorganic gyroid with exceptionally low refractive index from block copolymer templating. *Nano Lett.* **10**, 4994–5000 (2010).
44. Lin, T. C., Yang, K. C., Georgopanos, P., Avgeropoulos, A. & Ho, R. M. Gyroid-structured nanoporous polymer monolith from PDMS-containing block copolymers for templated synthesis. *Polymer* **126**, 360–367 (2017).
45. Yang, K. C. et al. Single gyroid-structured metallic nanoporous spheres fabricated from double gyroid-forming block copolymers via templated electroless plating. *NPG Asia Mater.* **11**, 9 (2019).
46. Yadav, L. D. S. In *Organic Spectroscopy* 7–51 (Springer Netherlands, 2005).
47. Lumerical Solution, Inc. (Mitacs, 2022).
48. Li, H. et al. A shifted double-diamond titania scaffold. *Angew. Chem. Int. Ed. Engl.* **56**, 806–811 (2017).
49. Wu, Y. H., Lo, T. Y., She, M. S. & Ho, R. M. Morphological evolution of gyroid-forming block copolymer thin films with varying solvent evaporation rate. *ACS Appl. Mater. Interfaces* **7**, 16536–16547 (2015).
50. Park, S. et al. Giant gyroid and templates from high-molecular-weight block copolymer self-assembly. *Sci. Rep.* **6**, 36326 (2016).
51. Saba, M., Wilts, B. D., Hielscher, J. & Schroder-Turk, G. E. Absence of circular polarisation in reflections of butterfly wing scales with chiral Gyroid structure. *Mater. Today. Proc.* **1**, 193–208 (2014).
52. Gan, Z., Turner, M. D. & Gu, M. Biomimetic gyroid nanostructures exceeding their natural origins. *Sci. Adv.* **2**, e1600084 (2016).
53. Stefik, M., Guldin, S., Vignolini, S., Wiesner, U. & Steiner, U. Block copolymer self-assembly for nanophotonics. *Chem. Soc. Rev.* **44**, 5076–5091 (2015).
54. Dolan, J. A. et al. Controlling self-assembly in gyroid terpolymer films by solvent vapor annealing. *Small* **14**, e1802401 (2018).